Thermoreflectance of LiF between 12 and 30 eV†

M. Piacentini,* D. W. Lynch, and C. G. Olson

Ames Laboratory–ERDA and Department of Physics, Iowa State University, Ames, Iowa 50010

(Received 12 January 1976)

The thermoreflectance spectrum of LiF between 12 and 30 eV was measured and several of the structures interpreted. The absorption-edge region is interpreted in terms of a Wannier exciton series converging to the fundamental band gap $\Gamma_{15} \to \Gamma_1$. Structure associated directly with the band gap is not manifest, so the Γ_{15}-Γ_1 energy is determined indirectly to be 14.2 ± 0.2 eV. The $n = 1$ exciton state generates the first strong structure in $\Delta\bar{\epsilon}$ and we suggest that the exciton-phonon interaction, along with a central-cell correction, can give a significant contribution to its binding energy. Structures at higher energy have been associated with the interband transitions $L_3' \to L_1$ and $L_2' \to L_1$ between the crystal-field-split valence band at L and the lower conduction band. The strong electron-hole interaction modifies the expected line shape and a hyperbolic exciton, associated with the transitions at L, may exist as an antiresonance in the continuum. A strong feature at 22.2 eV in $\Delta\bar{\epsilon}$ is associated with excitonic transitions at X involving the second d-like conduction band. The corresponding peak at 26.4 eV in $\Delta[\text{Im}(-1/\bar{\epsilon})]$ overlaps the "valence-band" plasmon at 24.6 eV. No evidence for double excitations is found around 25 eV in either $\Delta\bar{\epsilon}$ or $\Delta[\text{Im}(-1/\bar{\epsilon})]$. The $\Delta[\text{Im}(-1/\bar{\epsilon})]$ spectrum shows for the first time which structures in the energy-loss function are generated by longitudinal excitons and which by plasmons.

I. INTRODUCTION

LiF has its absorption edge at very high energy and is used as a window in far-ultraviolet spectroscopy to separate the sample chamber from the rest of the optical instrumentation. The study of its optical properties was delayed until rather recently, when windowless optical systems had been developed along with light sources emitting in the far ultraviolet up to 400 Å. Since then, the reflectivity[1-5] and the absorption[6,7] of LiF have been measured by several groups, at first using line sources,[1-4,6] then recently using the synchrotron-radiation continuum.[5] The optical data have been augmented by electron energy-loss (EEL) experiments.[8-11] Thus the spectrum of electronic transitions is fairly well known. The ϵ_2 spectrum[3-5] (where ϵ_2 is the imaginary part of the dielectric function $\bar{\epsilon} = \epsilon_1 + \epsilon_2$) shows a strong narrow peak at 12.6 eV, just above the absorption edge, followed by three broad bands at 14.5, 17.5, and 22.0 eV. (See Fig. 1.) The interpretation of this spectrum is still rather primitive. Sharp structures superimposed on broader features have been used to identify particular transitions in the case of semiconductors and other alkali halides,[12] but unfortunately the LiF ϵ_2 spectrum is smooth.[13]

Several energy-band calculations have been performed recently for LiF,[14] using different methods, and the results are in surprisingly good agreement with each other for the valence bands and the lower conduction band. However, disagreement is found for the calculated band gaps.

In particular, it was shown that *ab initio* Hartree-Fock calculations describe the crystal ground-state properties very well,[15] and, when correlation and relaxation effects are taken into account for describing the excited crystal,[16,17] the calculated band gap is in excellent agreement with the optical gap.[18] Thus, in the following, we shall refer to these calculations[15-17,19,20] which also give enough of the higher conduction bands to make a comparison with experiment possible.

The interpretation of the over-all spectrum is still controversial. The excitonic nature of the first peak in ϵ_2 was recently disputed.[19] The broad band at 23 eV was associated either with interband transitions around[3,4] X or with the simultaneous excitation of two fundamental excitons.[21,22] The states at X of d symmetry, may shift by several eV according to the computational method employed. Perrot[16] found them in the proper energy range to account for the observed peak while in the bands of Mickish *et al.*[17] they lie much higher, and the calculated ϵ_2 is structureless around 23 eV, in support of the double excitation mechanism.[21,22]

In spite of the strong electron-hole interaction in LiF, excitonic effects have been neglected in discussing its optical properties above the band gap. The binding energy E_b of the fundamental exciton is about 2 eV.[18] In this case the one-electron density of states should be completely modified by the electron-hole interaction for several E_b above the band gap,[23] thus throughout the interband absorption region. Excitonic effects have been recognized in the interband continuum
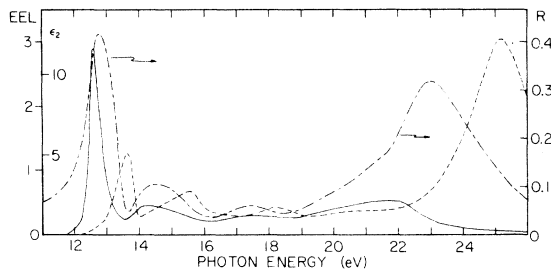
FIG. 1. Reflectance R (dash-dot), imaginary part of the dielectric function ϵ_2 (solid), and electron energy-loss function EEL (dashed) spectra for LiF. R is from Ref. 3 with data from Ref. 5 at higher energy. ϵ_2 and EEL were from a Kramers-Kronig analysis of R.

of semiconductors, where E_b is only some tens of millivolts.

Recently, the technique of modulation spectroscopy was applied successfully to the study of metals[24,25] and semiconductors[26] in the far ultraviolet. As is well known, features observed in the modulated spectra can be related only to particular transitions occurring around critical points of the Brillouin zone (or to plasma edges), while the dc spectra are dominated by the large background of noncritical transitions.[27] We thus measured the thermoreflectance (TR) spectrum of LiF throughout the fundamental interband absorption region (12–30 eV). Several new structures were observed for the first time. Excitonic effects have been found far above the absorption gap, but no evidence for double excitations around 22 eV is found. The roles of oscillator and plasmon peaks above the interband absorption region were clarified by studying the thermomodulation (TM) EEL function $\Delta(-1/\tilde{\epsilon})$.

In Sec. II we shall describe the experimental setup and the TM results, comparing them with other available optical data. In Sec. III we shall discuss in detail the excitonic region (12–15 eV). In Sec. IV we shall concentrate on the interband transitions involving the lower conduction band (15–20 eV). In Sec. V we shall analyze the structure at 23 eV, and finally, in Sec. VI, the longitudinal spectrum will be compared with the transverse one.

II. EXPERIMENTAL AND RESULTS

Synchrotron radiation emitted by the electrons orbiting in the storage ring Tantalus I of the Synchrotron Radiation Center, Physical Sciences Laboratories, University of Wisconsin, was used as a light source. The optical system is described in detail elsewhere.[28] A normal incidence 1-m McPherson 225 monochromator was used with a

gold-coated 1200-line/mm grating. The radiation reflected by the samples was detected with a windowless electron multiplier with a Be-Cu cathode.

It is important to note that, despite digital data handling, the electron multiplier was used in the current mode. In the counting mode, the limiting count rate of ~ 1 MHz limits us to measuring structures no smaller than $\Delta R/R \approx 10^{-3}$ for a 1-sec counting time. In the current mode, a greater photon flux could be used, corresponding to count rates of up to 100 MHz, and structures of 10^{-4} for 1-sec integrations.

The samples were indirectly heated. A molybdenum film of 10–30-Ω resistance was evaporated on a quartz plate attached to the cold finger of a liquid-nitrogen cryostat. A unipolar square-wave current of 1.5–3.5-W peak power flowed through the film, modulating its temperature. The samples were either single crystals cleaved as thin as possible prior to mounting on the heater or thin films directly evaporated on the Mo film. In both cases they were exposed to the atmosphere for only a few minutes. Two different frequencies were employed: 1.6 Hz with a conventional analog lock-in detection system and 0.1 Hz with a digital lock-in system. In the latter case the output of the electron multiplier was preamplified and then voltage-to-frequency converted. The pulses were counted with an SSR 1110 digital synchronous computer operated in the chop mode. The input signal is split into two different channels, A and B, according to a reference gate, properly phase shifted, provided by the voltage supplied to the heater. Channel A counts the pulses generated during the time the heater was on and channel B counts those when the heater was off. After a predetermined number of cycles, the counter displays the quantities $A - B$, proportional to the differential signal ΔI_R, and $A + B$, proportional to $2I_R$. The TR spectrum is given by $\Delta R/R = \Delta I_R/I_R = 2(A - B)/(A + B)$.[29] 6–10 cycles were enough to obtain good statistics (high signal-to-noise ratio) in a reasonable amount of time. At 0.1 Hz we observed a background signal due to the decay of the electron beam in the storage ring. At 1.6 Hz TR signals of the order of 10^{-5} were reproducible, while the sensitivity at 0.1 Hz was about 10^{-4}. On the other hand, at 0.1 Hz the temperature modulation was much larger and allowed us to extend the measurements to higher energies, where the light intensity was too small to use the lock-in. The average temperature at which the spectra were recorded was 200–250 K.

In Fig. 2 we display the TR spectra measured on a single crystal at 1.6 Hz (solid line) and on a thin film at 0.1 Hz. Except for the different intensities
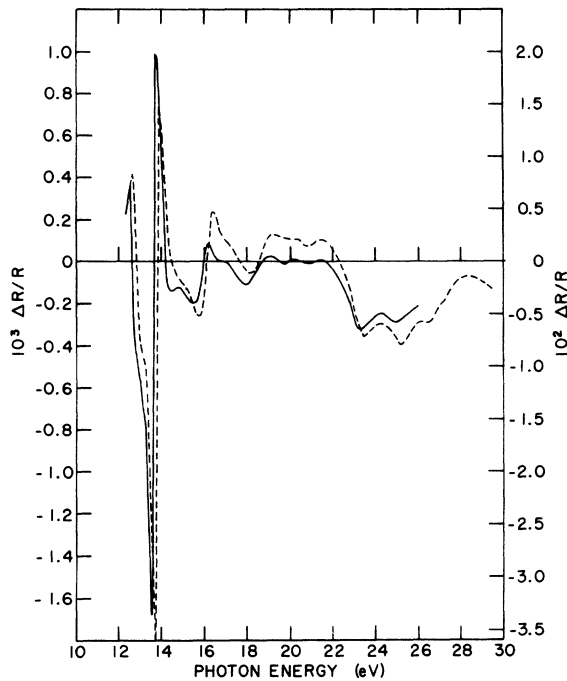
FIG. 2. Thermoreflectance spectrum of LiF. Solid line: single crystal, 1.6 Hz and 3.1-W modulation power (left scale). Dashed line: thin film, 0.1 Hz and 1.6-W modulation power (right scale).

the two spectra are very similar. The film spectrum does not show all the details resolved in the crystal spectrum and is shifted upward. The temperature modulation in the case of the single crystal was estimated to be about 0.4 K. Assuming that the intensity of the TM signal increases linearly with modulation amplitude, the dashed curve corresponds to a ΔT of about 10 K. The ideal conditions of a modulation experiment are approached in the limit of very small temperature variations ($\Delta T \rightarrow 0$). In this case the contributions to the measured signal come only from critical-point transitions and plasmons. When ΔT is large, the contribution from general transitions also becomes significant, resulting in a loss of detail. This effect is much more pronounced when the difference between two spectra measured at two different temperatures is calculated. The dashed spectrum of Fig. 2 is in very good agreement with the difference spectrum calculated by Rao.[5] Our TR spectra around the exciton region are very similar to the TR spectra of other alkali halides measured by Nosenzo et al.[30]

Comparing our TR spectrum (Fig. 2, solid) with the reflectivity of LiF,[1-5] we see that the feature between 12 and 14.5 eV corresponds to the exciton peak at 12.7 eV (Fig. 1) and the onset of the

next band, both of which shift to higher energies upon cooling. Structure between 15 and 16.5 eV seems to be associated with the dip in reflectivity at 16 eV. We find new features where the reflectivity shows a smooth band centered at 17.5 eV. We do not associate them with the fine structure observed by Stephan.[13] All the structure above 22 eV is related to the broad band peaking at 23 eV and is present in the data of Rao.[5]

The TR spectrum measured on the single crystal at 1.6 Hz was Kramers-Kronig analyzed to obtain the TM optical constants $\Delta\theta$, $\Delta\tilde{\epsilon}$, and $\Delta(-1/\tilde{\epsilon})$ $=\Delta L$. ($\Delta\theta$ is the Kramers-Kronig transform of $\Delta R/R$.) From 25 to 30 eV we used the thin-film data (Fig. 2, dashed curve) properly scaled. Above 30 eV we let $\Delta R/R$ go to zero smoothly at 40 eV. The influence of the extrapolation is small in differential Kramers-Kronig transformations.[31] We checked this by transforming only the data below 17 eV. In that portion of the spectrum the results did not change significantly. From $\Delta R/R$ and $\Delta\theta$, $\Delta\tilde{\epsilon}$ can be easily calculated using the normal-incidence relations

$$\Delta\tilde{\epsilon} = \sqrt{\tilde{\epsilon}}\,(\tilde{\epsilon}-1)\,d\tilde{r}/\tilde{r}, \tag{1a}$$

$$d\tilde{r}/\tilde{r} = \tfrac{1}{2}\Delta R/R + i\Delta\theta, \tag{1b}$$

$$\Delta L = \mathrm{Im}(\Delta\tilde{\epsilon}/\tilde{\epsilon}^2). \tag{1c}$$
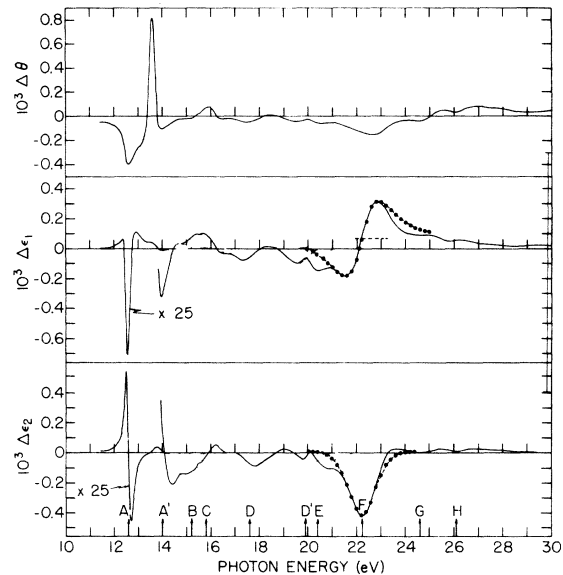
FIG. 3. Differential optical constants of LiF obtained by Kramers-Kronig analysis of the thermoreflectance spectrum of a single crystal, shown in Fig. 1. From top: $\Delta\theta$, $\Delta\epsilon_1$, and $\Delta\epsilon_2$, respectively. The dotted lines around 22 eV in $\Delta\epsilon_1$ and $\Delta\epsilon_2$ are calculated spectra (see text).

Here we used complex notation for the optical constants. $\tilde{r}$ is the Fresnel coefficient for reflectivity at normal incidence, given by $\tilde{r} = R^{1/2}e^{i\theta}$ $= (\sqrt{\tilde{\epsilon}} - 1)/(\sqrt{\tilde{\epsilon}} + 1)$. There is some discrepancy in the literature on the magnitude of $\tilde{\epsilon}$ and on the energy of some of the peaks.[3-5] This discrepancy also affects the calculated $\Delta\tilde{\epsilon}$. We Kramers-Kronig transformed the LiF reflectivity data available in the literature (Fig. 1). The best results were obtained with the data of Roessler and Walker.[3] We therefore used their data for $\tilde{\epsilon}$ in Eqs. (1a–1c). The TM spectra thus obtained are shown in Fig. 3.

III. EXCITON REGION (12–15 eV)

The TR spectrum between 12 and 15 eV is very similar to the first energy derivative of the reflectivity, indicating that the main effect of temperature is to shift the reflectivity structure to higher energies upon cooling. This result is in agreement with the measurements at different temperatures of Watanabe et al.[7] and of Rao.[5]

A pronounced shoulder is present on the low-energy side of the strong negative peak at 13.5 eV. The exciton peak of LiF, as well as that of the other alkali fluorides, actually shows an asymmetry in the reflectivity[1-5] and transmission[6,7] (optical density) spectra. Due to this double structure, it has been speculated that two different electronic transitions occur here.[3] One of us has shown recently that the peak at 12.62 eV of the ϵ_2 spectrum of LiF is formed by a single oscillator.[18] The line shape is described by an asymmetric Lorentzian function,

$$\epsilon_2(E) = \frac{\sigma_2}{2E} \frac{\Gamma + A(E - E_p)}{(E - E_p)^2 + \Gamma^2}, \qquad (2)$$

above the absorption threshold. The low-energy tail falls off exponentially according to the Urbach rule.[32] In Eq. (2) E_p is the oscillator energy, Γ is the half width at half maximum, A is the asymmetry parameter, σ_0 is the line intensity, related to the oscillator strength f by $\sigma_0 = f(\hbar\omega_p)^2/2$, and ϵ_c is an effective dielectric constant. For a single oscillator, $\epsilon_c = 1$. Since here we are below all interband transitions, we use $\epsilon_c = \epsilon_\infty = 1.92$. With this value of ϵ_c and with $\Gamma = 0.19$ eV, $\sigma_0 = 13.13$ eV^2, $A = 0.33$, and $E_p = 12.59$ eV,[18] both the real and imaginary parts of $\tilde{\epsilon}$ can be fitted. This implies that a single electronic process is responsible for the reflectivity peak at 12.7 eV. The double structure of the reflectivity peak arises from the different energies at which ϵ_1 and ϵ_2 peak. This result is fully confirmed by the TM experiment. We calculated $\Delta\tilde{\epsilon}$ and $\Delta R/R$ from Eq. (2), shifting the peak energy and allowing a small

variation of the broadening, according to

$$\Delta\tilde{\epsilon} = \tilde{\epsilon}(T + \Delta T) - \tilde{\epsilon}(T) = \left(\frac{\partial\tilde{\epsilon}}{\partial E_p} \frac{dE_p}{dT} + \frac{\partial\tilde{\epsilon}}{\partial\Gamma} \frac{\partial\Gamma}{\partial T} \right)\Delta T.$$

$$(3)$$

Equation (3) actually represents the first term of a Taylor-series expansion for $\tilde{\epsilon}$ and it is valid only for very small temperature variations. In Fig. 4 we display an expanded plot of $\Delta\tilde{\epsilon}$ between 12 and 15 eV (solid curve). The dots correspond to the calculated spectrum using Eqs. (2), (3), with the values of the parameters given above. In Fig. 5 we compare the experimental $\Delta R/R$ (solid line) with the calculated one. The agreement between the measured and calculated spectra is very good, especially considering that the parameters used in Eq. (2) were the same as those determined for the ϵ_2 spectrum of Roessler and Walker,[3] rather than determined directly from the present measurements. The double feature of $\Delta R/R$ is reproduced even though we started with only one oscillator. From the fit, we find that $\Delta\Gamma = 0.1$
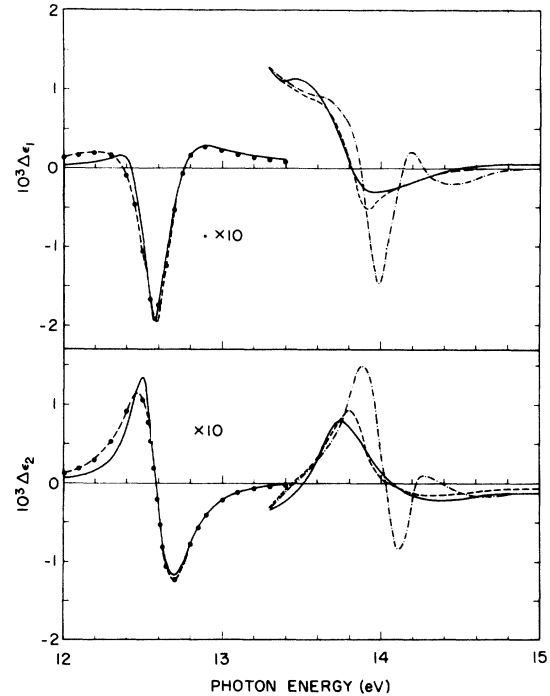
FIG. 4. $\Delta\epsilon_1$ and $\Delta\epsilon_2$ for the exciton region (solid lines) compared with the calculated spectra assuming modulation occurs by a shift and a broadening of the structure. Dotted line: contribution from the $n = 1$ exciton state. Dash-dot line: curves calculated including the $n = 2, \ldots, \infty$ states and the continuum with the parameters obtained in the fit of Ref. 18. Dashed line: total contribution, calculated using different parameters, as discussed in the text.
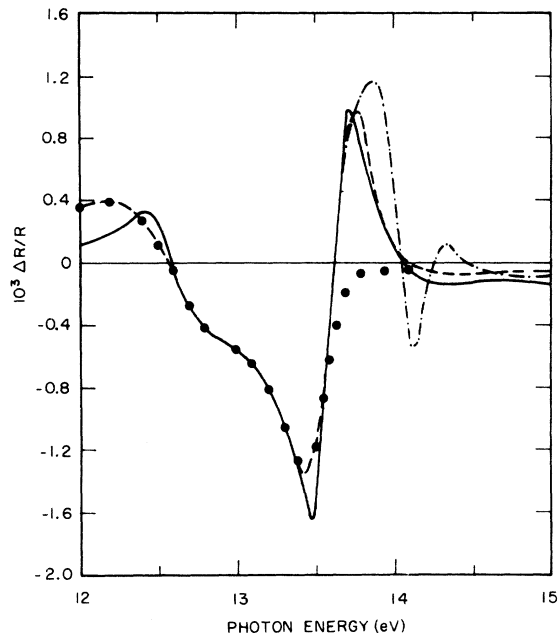
FIG. 5. Thermoreflectance spectrum around the first exciton peak of the single crystal compared with calculated curves. Dotted line: contribution from the $n = 1$ exciton state obtained by shifting and broadening a single asymmetric oscillator at 12.59 eV. The contribution from the $n = 2, ..., \infty$ states and the continuum is included using the parameters of Ref. 18 (dash-dot line) and a different set of values (dashed line). The experimental spectrum is the solid line.

meV and $\Delta E_p = 0.3$ meV. Comparing the value of ΔE_p obtained for the single-crystal TR spectrum with a temperature coefficient of 0.8 meV/K, which can be determined from the data of Watanabe et al.[7] and of Rao,[5] allows us to obtain indirectly a temperature modulation of 0.4 K on the sample surface.

In Ref. 18 it was shown that the experimental ϵ_2 curve above 13.6 eV could be fitted with the exciton effective-mass approximation[23] applied to the $n = 2, ..., \infty$ states and the continuum. The strong peak at 12.6 eV was taken as the $n = 1$ state, described by Eq. (2). The nth state also was described by Eq. (2) with an intensity σ_0/n^3 and peak energy $E_p = E_g - G/n^2$, where G is the exciton effective Rydberg. E_g and G were the free parameters in the fit, so that central cell corrections for the $n = 1$ state were allowed. Otherwise, the relation $E_{n=1} = E_g - G$ related E_g and G. The best fit was obtained with $E_g = 14.5$ eV and $G = 2.09$ eV, but the calculated $n = 2$ line was resolved from the continuum. It was observed that a smaller value of the ratio G/Γ would make the $n = 2$ state merge into the continuum. In such a case, the value of σ_0 for the higher excited states would have to be reduced.

We made use of the above results and calculated the TM spectra for the higher excited states, assuming that the shift was due only to a variation ΔE_g of the gap energy, with $\Delta E_g = \Delta E_p$ found previously. The same $\Delta \Gamma$ was used as well. The Appendix discusses the functional forms for $\tilde{\epsilon}$, both below and above the M_0 critical point. In Figs. 4 and 5 we compare the experimental $\Delta \epsilon_2$ and $\Delta R/R$ with the spectra calculated using $E_g = 14.15$ eV, $G = 2.09$ eV (dash-dot line), and $E_g = 14.15$ eV, $G = 1$ eV, and σ_0 scaled by 0.5 with respect to the $n = 1$ value (dashed line).[33] The $n = 2$ line is completely resolved in the former curve, as expected, since it corresponds to the fit of ϵ_2 in Ref. 18. With this exception, the general experimental shape is reproduced. Better agreement is obtained for the other curve. We therefore suggest that the structure at 12.6 eV corresponds to only the $n = 1$ exciton state, and that the structure from 13.6 to 14.7 eV corresponds to the continuum formed by the other exciton states and the interband continuum. Due to the uncertainty in fitting the line shape, it is not possible to determine accurately the position of the band gap and the effective Rydberg. According to our model, structure associated uniquely with the interband gap is not manifest, as in the TR[30] and electroreflectance[34] spectra of other alkali halides. Thus we cannot give an experimentally determined value of the band gap, but we believe that it lies between 14.0 and 14.5 eV, i.e., 14.2 ± 0.2 eV. The binding energy E_b of the $n = 1$ state correspondingly ranges from 1.4 to 1.9 eV.

The use of the effective-mass approximation is justified for the $n = 2, ...$ states, since the hydrogenic radius is much larger than the lattice constant. The $n = 1$ state radius, however, is comparable with the nearest-neighbor distance. In such a case, large central cell corrections are expected. These result in a shift of the peak energy from the hydrogenic value $E_{n=1} = E_g - G$, in a shift of oscillator strength from the other lines and the continuum into the $n = 1$ state, and in a larger electron-phonon interaction. Assuming that the values of E_g and G used in calculating the dashed curve of Fig. 4 are the closest to the true values, we find that the energy difference δE_b between the true binding energy E_b and the hydrogenic binding energy G of the $n = 1$ state is approximately 0.5 eV, and that it also has gained oscillator strength by a factor of $(E_b/G)^{3/2} = 1.7$ (see Appendix), in agreement with the above considerations.

Mickish et al.[17] calculated the ϵ_2 spectrum of LiF. Their band-gap energy (14.3 eV) is in excellent agreement with our results. They also included excitonic effects, using the one-band-

one-site approximation. Their potential allowed for only one bound state. The wave function of this state is formed mostly from states around L, where the conduction-band density of states peaks. The strong electron-hole interaction creates the bound state in the band gap, with binding energy 1.8 eV. It is associated with the $n = 1$ exciton state generating the peak in ϵ_2 at 12.6 eV.[3] Note that this result is in agreement with the general theory of Toyozawa et al. on the metamorphism of critical points.[35] Mickish et al.[17] also postulated the existence of higher excitonic states as resonances in the continuum, the series limit being the gap at L (17 eV), in order to explain the broad band peaking at 14.5 eV.[3-5] Our interpretation, based on the TM results discussed previously, does not agree at all with the analysis of Mickish et al., since we find that the whole exciton series lies below, and converges to, the band gap at $\Gamma (\sim 14.5$ eV). We are able to explain, on the same basis, part of the structure above 13.6 eV. We note that Antoci and Nardelli[36] calculated the exciton energies of KI and RbI using a different single-site formalism that that used by Mickish et al. for the $n = 1$ exciton state, and using the effective-mass approximation for the other states. They obtain good agreement with the TM data of Nosenzo et al.[30]

The deviation from the Wannier model for the $n = 1$ exciton state also can be due in part to the exciton-phonon interaction.[37,38] In the case of weak coupling, represented by the condition $\alpha = skT/B^2 < 1$, the exciton line shape is given by the asymmetric Lorentzian function Eq. (2).[37,38] Here α is the coupling constant, B the half width of the exciton band, k the Boltzmann constant, and s represents the energy gain of the localized exciton due to the lattice vibrations. The unperturbed exciton energy E_0 is shifted by the exciton self-energy Σ in the phonon field, so that, in Eq. (2), $E_p = E_0 - \Sigma$. This results in stronger binding for the exciton. Also the oscillator strength is increased by the exciton-phonon interaction.[37] All the parameters of the line shape, Eq. (2), depend on α and thus on temperature. We shall use here the simple expressions given by Sumi,[38] aware of the limits of his calculations:

$$\Sigma/B = 2\alpha, \quad \Gamma/B = 2\alpha^2, \quad A \sim \text{const}, \tag{4}$$

from which we derive the relation

$$(d\Gamma/dT)(d\Sigma/dT)^{-1} = 2\alpha. \tag{5}$$

Using for $d\Sigma/dT$ half of the value determined for dE_p/dT,[39] we obtain $\alpha = 0.3$ for LiF. The condition of weak coupling is satisfied again. We also have $B \sim \Gamma/2\alpha^2 = 0.9$ eV, and $\Delta = 12$. The value of Σ is the same as that of δE_b as if the

exciton energy E_0 were the hydrogenic one. However, we believe this coincidence is only fortuitous. First, the value given for δE_b is not accurate but only indicative. The same is true for the value of $d\Sigma/dT$ used in Eq. (5). Third, in the region of our values of α, the relations between the line-shape parameters and the temperature Eq. (4) change. Nevertheless, the contribution of Σ to the binding energy of the exciton might be significant, although perhaps not as large as 0.5 eV. This effect has not been considered previously in the interpretation of optical data for LiF.

IV. INTERBAND REGION (15-21 eV)

The TR spectrum measured on a single crystal at 1.6 Hz revealed several new structures between 15 and 20 eV, structures not seen in the reflectivity of LiF.[1-5] Stephan[4] observed two peaks at 17 and 18 eV, not confirmed by other measurements, which do not have any counterpart in our data. The two features at 15.4 and 15.6 eV could be resolved only by averaging several spectra taken with very small temperature variations, and represent the limit of our sensitivity. Figure 6 shows $\Delta\epsilon_1$ and $\Delta\epsilon_2$ in this region. Decompositions of the structures have been sketched in order to help in identification.

We first discuss the features D and D' which appear as two negative peaks in both $\Delta\epsilon_1$ and $\Delta\epsilon_2$.
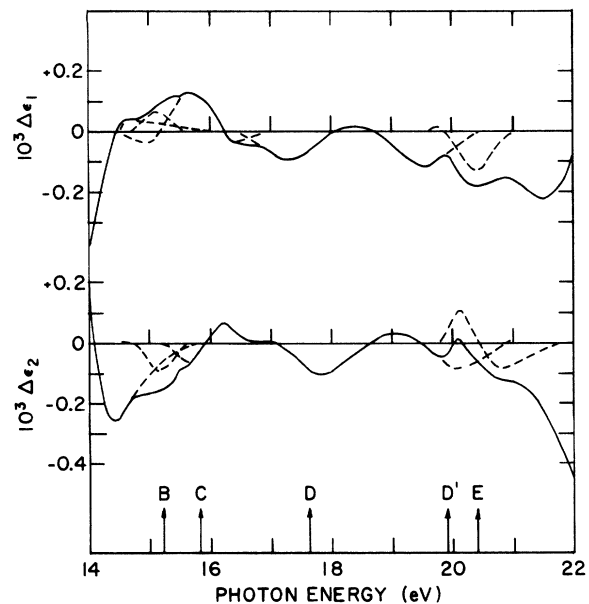
FIG. 6. Expansion of part of Fig. 2. The dashed lines show a rough decomposition of the spectra into components, marked by arrows at the bottom.

Such behavior suggests that they originate from transitions involving a Van Hove singularity,[40] of the same type for both D and D'. (The energy of the singularity is the average energy of the negative peaks, nearly the same in $\Delta\epsilon_1$ as in $\Delta\epsilon_2$.) For D we find 17.60 eV. D' is partially mixed with the next feature, especially in $\Delta\epsilon_2$. By analogy with the feature D in $\Delta\epsilon_1$ we determine the energy of 19.9 eV for D'. The identification of the type of singularity is more difficult. Assuming for the moment that the TM spectrum arises from modulating the singularity energy rather than the broadening parameter, we can associate D and D' either with two M_0 singularities shifting to lower energies or with two M_2 singularities shifting to higher energies upon cooling.[40]

The ϵ_2 spectrum calculated by Mickish et al.[17] shows two peaks around 17.3 eV associated with transitions along Λ ($\Lambda_3 - \Lambda_1$), for which a large joint density of states exists near L. These peaks were associated with the structures observed by Stephan.[4] A much weaker "replica" around 19.5 eV, due to transitions $\Lambda_2 - \Lambda_1$, is also predicted.[17] Even if the structure D does not correspond to any of those observed by Stephan, we associate it with the $\Lambda_3 - \Lambda_1$ transitions. The energy difference between D and the energy gap is about 3.3 eV, in agreement with the theoretical value.[15-17] Similarly, D' corresponds to the transitions $\Lambda_2 - \Lambda_1$ between the crystal-field-split valence band and the lower conduction band. The separation between D and D' of 2.3 eV agrees with the calculated splitting of the valence band at L.[15-17] It also agrees with the experimental splitting of the valence bands measured in photoemission.[41,42]

Even if an M_0 critical point cannot be ruled out as a possible source for the structures D and D', we believe it is very unlikely. The main reason is that the energy gaps in LiF tend to increase at lower temperatures, owing to lattice dilatation.[43] The temperature behavior of the optical properties of LiF has several points in common with that of the other alkali halides and zinc-blende semiconductors.[40] The reason is based on the fact that the lower conduction band in all these materials is very similar.[12] First, for all of them it is formed mostly from s-like states of the cation, except at L, where the wave function is a mixture of p-like states of the cation and s-like states of the anion, owing to inversion symmetry. The consequence of this is that L_1 tends to be pulled down with respect to Γ_1, because it does not feel the repulsive contribution to the pseudopotential of the s-like core states. This repulsive term is stronger for large overlap of the core state with the conduction states.

Thus the conduction band along Λ is almost flat near L_1 in LiF,[15-17] while it develops a maximum and forms a local minimum at L in other alkali halides and in the semiconductors.[12] The joint density of states for transitions from the valence band to the lower conduction band should have an M_1 critical point along Λ and, eventually, an M_0 critical point at L. In the zinc-blende semiconductors the M_1 critical point was identified with the peak E_1 in ϵ_2.[12] Modulation experiments supported such an interpretation. In particular, TR measurements have been interpreted assuming only a shift of the E_1 structure to higher energies upon cooling.[40] In analogy with this analysis, we neglected the modulation of the broadening, as mentioned above. Again, in the case of the zinc-blende semiconductors, the modulation spectra have shown that the M_1 critical-point line shape is modified by the electron-hole interaction, the actual line shape being an admixture of M_1 and M_2 structures,[40] in agreement with the theory of Toyozawa et al.[35] on the metamorphism of Van Hove singularities. In LiF the electron-hole interaction is much stronger than in semiconductors and the metamorphism of the M_1 structure into an M_2 structure may be complete. The structures D and D' probably do not correspond to real M_2 critical points. In addition to the theory of Toyozawa et al.,[35] it is well known that, according to the effective-mass approximation, the electron-hole interaction tends to wash out any structure associated with M_2 critical points which, therefore, are hard to observe, while it tends to enhance the M_1 features.[44]

The strong electron-hole interaction might even give rise to bound states below the M_1 threshold (hyperbolic excitons). In the spectra of Fig. 6 we see a structure C which seems to have a line shape similar to that of the fundamental exciton, except for the inverted sign. This structure can be reproduced by shifting either a peak in ϵ_2 to lower energies or a dip to higher energies upon cooling. Either case seems to follow the behavior of the D and D' features. Thus a possible assignment for C is a hyperbolic exciton associated with the M_1 critical-point transition D. Its energy, 15.9 eV, is in agreement with the energy of the dip in ϵ_2. A bound-state degenerate with a continuum occurs in many physical systems and has been extensively studied.[45-48] The line shape has a dip as a consequence of the interference of the bound-state wave function with the continuum wave functions. If either the bound-state lifetime or the transition probability for exciting the bound state is small, the bound state does not show up in the excitation process as a peak, but the dip still remains to indicate its

presence.[45] The situation which usually occurs is that of a bound state of a certain configuration of the system which is degenerate with the continuum of a different configuration, such as the discrete spectrum of double excitations degenerate with the single-electron ionization continuum of an atom or an exciton state associated with the minimum of a higher conduction band. In such cases the bound state does not lose its identity and generates an absorption peak. The hyperbolic exciton exists because of a topologically favorable condition of the interband continuum. In this case there are not two different configurations of the system, either of which can be excited. The exciton is interacting with its own continuum and thus its lifetime might be small enough to almost destroy the resonance. Toyozawa et al.[35] gave, in a very general form, the conditions for this to occur. We thus believe that the bound state associated with the M_1 critical point at L in LiF gives rise to the dip in ϵ_2 at 16 eV rather than to a peak. Its binding energy is 1.7 eV, comparable with that of the fundamental exciton. The interpretation of structure C suggested here is again in disagreement with the calculation of Mickish et al. for the fundamental exciton discussed in Sec. III.

The data presented in Fig. 6 show more structures at about 15.5 and 20.5 eV for which no assignment was attempted.

V. HIGHER INTERBAND REGION (20–30 eV)

The main structure in $\Delta\mathcal{E}$ at 22.2 eV (Fig. 3) corresponds to the peak in ϵ_2 at 21.7 eV.[3] Representing the ϵ_2 structure with a symmetric Lorentzian function given by Eq. (2) with $A = 0$ and with $E_p = 22.2$ eV, $\Gamma = 1.2$ eV, and $\sigma_0 = 54.6$ eV^2, we calculated the TM spectrum by means of Eq. (3). The result, shown in Fig. 3 by the dots, was obtained considering only a temperature modulation of the linewidth, with $\Delta\Gamma = 0.23$ meV and with no shift at all of E_p. A constant positive background was added to $\Delta\epsilon_1$ and the agreement achieved is very good.

Miyakawa[21] and Devreese et al.[22] suggested that the structure in ϵ_2 at 21.7 eV, as well as the EEL peak at 25 eV, are due to a resonant state of the electronic polaron, i.e., to the simultaneous creation of two excitons. This process generates an absorption band with a steep threshold at about twice the exciton energy E_0, reaching a maximum at about $2.2E_0$. The corresponding peak in the loss function should lie about 2 eV above the peak in ϵ_2, as actually occurs in several alkali halides, including LiF. The ϵ_2 spectrum calculated by Mickish et al.[17] is structureless between 20 and

25 eV, in support of this interpretation, which however, is not totally satisfactory (Fig. 1). The strength of the absorption structure was calculated using different approximations[21,22,49] and was found to range from being comparable with, to being much weaker than, the strength of the first exciton. In other words, doubt exists about the possibility of detecting it. Moreover, at least one of the two electron-hole pairs which are created corresponds to a "quantum" of the electronic polarization field, which is a longitudinal exciton.[50,51] The absorption peak then should be at $E_{0T} + 1.2E_{0L} = 28.8$ eV, while the experimental value is 23 eV. Here E_{0L} and E_{0T} are the energies of the longitudinal and transverse exciton, respectively. We believe that our results give experimental evidence that the double excitation mechanism[21,22] is not the principal source of the structure in ϵ_2 at[3] 21.7 eV and in EEL at 25 eV.[8-11] In fact according to this model, the absorption band should follow the behavior of the fundamental exciton upon cooling; i.e., it should shift to higher energy by an amount twice ΔE_p found in Sec. III. The change of the line width should give only a minor contribution. This is just the opposite of what we observe. Lapeyre et al.[52] reached conclusions similar to ours for KCl by means of photoemission spectroscopy.

The LiF energy bands[15-17] show that transitions to the lower conduction band should not give any significant structure to ϵ_2 above 20 eV. The next conduction band, of d character, has a minimum at X (X_3). Excitons associated with X_3 are considered responsible for several sharp absorption peaks far in the continuum in the case of other alkali halides.[4,7,53,54] In LiF X_3 lies fairly high in energy and no sharp peak appears in the absorption spectrum. The identification of transitions to X_3 becomes a challenge. Several assignments for the structure at 21.7 eV in ϵ_2 have been proposed but mostly on a speculative basis. It is difficult to support or disprove any of them. We feel that it probably arises from transitions at and around $X_5' \rightarrow X_3$. First, recently Perrot[16] and Euwema et al.,[15] using the Hartree Fock method, found the $X_5' \rightarrow X_3$ gap at about 8.5 eV above the fundamental gap $\Gamma_{15} \rightarrow \Gamma_1$, in fairly good agreement with the position of the high-energy peak in ϵ_2.[3-5] Second, on the Brillouin-zone boundary around X the bands are almost flat. Thus a large joint density of states is expected which should approach a two-dimensional logarithmic singularity. Third, we find a very small temperature dependence of the transition energy, as in the case of the X_3 excitons observed in the other alkali halides.[4,7,53,54] Finally, no strong partner structure, which might correspond to the $X_4' \rightarrow X_3$

transitions originating from the crystal-field-
split valence band, is observed at higher energies.
This is in agreement with the fact that the $X_4' - X_3$
transitions are dipole forbidden. Actually, two
weak minima exist in $\Delta\epsilon_2$ at 24.6 and 26.1 eV
(G and H in Fig. 3). The first one might corres-
pond to transitions occurring at general points
of the Brillouin zone around $X_4' - X_3$, which there-
fore are allowed, but with small oscillator
strength. The 2.4-eV splitting of the X_5' and X_4'
levels thus determined is in good agreement with
theoretical calculations.[15-17]

So far we have discussed the observed features
in terms of interband transitions only. However,
the observed line shape does not suggest critical
point transitions[40] but rather the broadening of a
peaked structure, which might be due to a peak
in the joint density of states as mentioned above.
In LiF the electron-hole interaction is strong
and modifies the one-electron picture as discussed
in Sec. IV. An excitonic transition, associated
with the band minimum X_3, could be responsible
for the observed features as well. Watanabe
et al.[7] have found the the energy of the X_3 exciton
observed in the other alkali fluorides is linearly
related to the inverse of the lattice constant. Ex-
tending this relationship to LiF, the exciton should
be at 21 eV, a little lower than the experimental
structure in $\Delta\epsilon_2$ at 22.2 eV. Similarly, we can
interpret the structure at 24.6 eV as the exciton
associated with the $X_4' - X_3$ gap. Most of the argu-
ments used to identify the peak at 21.7 eV in ϵ_2
with transitions at X are still valid. In the present
case, the calculated interband gap $X_5' - X_3$ is in
closer agreement with experiment, which now
gives the energy of a bound state below the con-
tinuum. The width of the exciton line in LiF is
rather large. But the exciton energy is very close
to the top of the conduction band, and this pro-
vides a strong decay mechanism. The lower X_3
is with respect to Γ_1 the sharper the exciton line
should appear. This trend seems confirmed by
the spectra of other alkali halides.[4,7,53,54]

VI. LONGITUDINAL SPECTRUM

The energies of the longitudinal resonances are
given by the peaks in the energy-loss function
$Im[-1/\epsilon(\vec{q}, \omega)]$. In the following we shall compare
EEL data with optical data so that we shall as-
sume the limit of negligible transferred momentum
$\vec{q}$ for the former. From the spectra of $\tilde{\epsilon}$, $\Delta\epsilon_1$,
and $\Delta\epsilon_2$ we also calculated the TM differential
electron energy-loss function ΔL shown in Fig. 7
for LiF. This spectrum is characterized by two
main features, the first at 13.5 eV and the second
at 25 eV. A weaker negative peak appears at
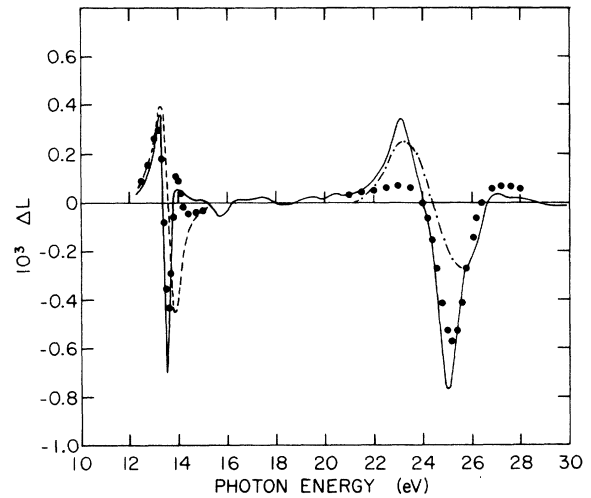
FIG. 7. Differential energy-loss spectrum of LiF. The
dotted curve around 13.5 eV was obtained from the
calculated spectrum of $\Delta\tilde{\epsilon}$ shown in Fig. 3 for the
exciton region. The dashed curve corresponds to the
contribution given by the $n = 1$ exciton state only. The
dotted curve around 25 eV was obtained from the calcu-
lated $\Delta\tilde{\epsilon}$ shown in Fig. 3 (dotted line). The dash-dot
curve sketches the contribution to the thermomodulation
spectrum from the plasma resonance of the valence
electrons.

15.7 eV.

The spectrum of the longitudinal excitations in
insulators was discussed extensively by Miya-
kawa.[55] Strong structures occur at the excitation
energy of the longitudinal excitons, which are
separated from the transverse excitons by[55,56]

$$E_{lT} = E_{0L} - E_{0T} = \frac{(\hbar\omega_p)^2 f}{2\epsilon_c E_{0T}}.\tag{6}$$

ϵ_c is the same effective dielectric constant as in
Eq. (2), but evaluated at the energy E_{0T}, ω_p is
the valence-band free-electron plasma frequency,
and f is the oscillator strength. The longitudinal
spectrum of interband transitions forms a band
of less prominent structures similar to those
present in the optical spectrum. In a two-band
model, a third type of longitudinal resonance may
exist above all the interband energies, provided
these are strong enough. This resonance occurs
where ϵ_1 crosses zero with positive slope in a
region of low absorption. In many respects it
can be identified with the shifted plasma resonance
of the valence electrons.[55] The free-electron
plasma frequency is shifted by the presence of
nearby interband transitions at higher and lower
energies.

The first structure in ΔL around 13.5 eV cor-
responds to the fundamental longitudinal exciton

series converging to the band gap. Using $\Delta\bar{\epsilon}$ calculated for the transverse exciton structure as described in Sec. III, we calculated the TM ΔL function shown by the dotted line in Fig. 7. The calculated ΔL for the first exciton state only, which gives a structure separated from the higher members of the series in $\Delta\epsilon_2$, has a dispersion-like line shape crossing zero at 13.5 eV (dashed line in Fig. 7). This result is expected since it derives from the thermal shift of the $n = 1$ line. Only by including the higher exciton states, can the calculated ΔL spectrum agree with the experimental curve. Using the optical dielectric constant $\epsilon_\infty = 1.92$ for ϵ_c in Eq. (6), the longitudinal-transverse splitting for the first line is 1.0 eV, in good agreement with the experimental value of 0.9 eV. In the effective-mass approximation, the oscillator strength of the higher exciton states decreases as $1/n^3$ and thus so does E_{LT}. Finally, the interband gap should not be shifted in the longitudinal spectrum.[57,58] The longitudinal exciton series is more compressed than the transverse one so that the $n = 1$ structure does not appear separated as it does in ϵ_2. The behavior of the longitudinal spectrum gives further support to our explanation of the absorption-edge region of LiF (see Sec. III): The exciton states are all below and converge to the fundamental gap $\Gamma_{15} - \Gamma_1$.

The negative peak in ΔL at 15.7 eV corresponds to the feature in $\Delta\epsilon_2$ at 15.8 eV and is in agreement with the peak in the EEL spectrum at 15.5 eV.[10] The TM ΔL spectrum originating from interband transitions shows no significant structure, while the EEL spectrum has a peak at[10] 18.1 eV (see the region between 16 and 20 eV in Fig. 7). The "strength" of the negative peak at 15.7 eV supports the suggestion of an excitonic effect in this region. The exciton manifests itself as an antiresonance in the continuum rather than as a peak. The antiresonance may be considered as a peak with a negative effective oscillator strength[35] which, introduced into Eq. (6), gives $E_{LT} < 0$ as found experimentally.

The next feature around 25 eV was discussed in detail in a previous paper[59] and we summarize here the conclusions. Its doublet structure, observed also in the EEL spectrum,[11] originates from the near degeneracy of a plasma resonance at 24.5 eV and a longitudinal "oscillator" at 25 eV. This assignment of the two features reverses the previous assignment of Gout and Pradal.[11] The shift of the plasma frequency to higher energy at lower temperatures gives the dispersion-like structure, sketched by the dash-dot line in Fig. 7. In the free-electron approximation, the shift originates from the variation of the density

of electrons due to the lattice dilatation. Neglecting broadening this yields

$$\Delta\epsilon_1 = -2\frac{\omega_p^2}{\omega^2}\frac{\Delta\omega_p}{\omega} = 3\frac{\omega_p^2}{\omega^2}\frac{\Delta l}{l}. \qquad (7)$$

$\Delta l/l$ is the linear thermal-expansion coefficient. In the case of LiF, $\Delta l/l = 0.35\times10^{-4}$, $\hbar\omega_p = 22.4$ eV for 6 valence electrons, so that at about $E = \hbar\omega_p$ and for $\Delta T \approx 0.4$ K, Eq. (7) gives $\Delta\epsilon_1 = 0.4 \times10^{-4}$. In Sec. V we found that, in order to obtain best agreement between the calculated $\Delta\epsilon_1$ and the experimental one for the structure at 22.2 eV, we had to add a positive background of 0.6×10^{-4}, the origin of which is now clear.

The broadening of the peak in ϵ_2 at 22.2 eV gives the negative peak in ΔL at 25 eV, as shown by the dotted curve calculated using the results of Sec. V. Using for ϵ_c the value of 0.85, corresponding to the constant difference between the experimental ϵ_1 and the calculated oscillator term above 24 eV, the transverse-longitudinal splitting of the oscillator is in agreement with the measured one. Once again the longitudinal spectrum seems to support the assignment given previously to a corresponding structure in ϵ_2. The peak in ϵ_2 at 22.2 eV originates from an exciton rather than from a high joint density of states. The 25-eV ΔL peak is the longitudinal exciton corresponding to the 22.2-eV transverse exciton, probably associated with $X_5' \rightarrow X_3$.

VII. SUMMARY AND CONCLUSIONS

We measured the thermoreflectance spectrum of LiF between 12 and 30 eV, finding several new structures in comparison with direct reflectivity[1-5] or absorption spectra.[6,7] In Table I we summarize the energies of the features we observe in $\Delta\bar{\epsilon}$ and our assignment. We also give the theoretical transition energies as obtained from band-structure calculations. In some cases we arbitrarily shifted the bands rigidly in order to match the experimental value of the band gap. Figure 8 summarizes the "experimental band structure."

The first strong structure was associated with the lowest bound state of an excitonic series. All the other states lie below the fundamental gap and converge to it, forming a continuum below 14.5 eV. This result does not confirm the picture[17] in which the exciton series originates from states around L, and only the first term lies in the band gap, all the others forming the broad peak at 14.5 eV in the ϵ_2 spectrum. We could not identify in the TM spectrum a structure associated with just the band gap $\Gamma_{15} - \Gamma_1$. The gap energy thus is determined indirectly, fitting ϵ_2 and TM data, to be between 14.0 and 14.5 eV and will certainly

TABLE I. Energies[h] of the structures observed in the thermomodulation $\Delta\mathcal{E}$ spectrum (Col. 1) and our assignment (Col. 2) compared with calculated interband gaps (Cols. 3–6). In the case of transitions terminating at the same final state but starting from the crystal-field-split valence band, the splitting of the valence bands is given too. All energies are in eV.

Structure and energy	Present assignment	Perrot[a] HFC[e]	Mickish et al.[b] HFC[e]	Euwema et al.[c] HF[f]	Laramore Switendick[d] HPW[g]
A 12.59	$n = 1$ exciton		12.3		
A' 14.0	$n = 2, ..., \infty$ and exciton continuum		$>\Gamma_{15}\Gamma_1$		
14.2 ± 0.02	Fundamental gap $\Gamma_{15} \rightarrow \Gamma_1$	14.2	14.1	14.2[h]	14.2[h]
B 15.0					
C 15.8	Hyperbolic exciton				
D 17.6	M_1 singularity[j] $\Lambda_3 \rightarrow \Lambda_1$	17.31	16.87	16.32	16.6
D' 19.9	M_1 singularity[j] $\Lambda_2 \rightarrow \Lambda_1$	18.94	19.16	19.02	18.4
	$\Lambda_2 \, \Lambda_3 = 2.3$	1.63	2.3	2.7	1.8
E 20.5					
F 22.2	Exciton $X_5'X_3$[k]	22.88	25.10	22.57	23.06
G[l] 24.6	Exciton $X_4'X_3$	24.16	27.95	24.69	24.76
	$X_4'X_5'$ 2.4	1.28	2.85	2.12	1.7
	$X_5'X_1$	24.39	26.36	24.47	23.72
H[l] 26.1	$X_4'X_1$	25.67	29.15	25.6	25.35
	L_3L_3	26.96	26.57	25.52	–

[a] Ref. 16.

[b] Ref. 17.

[c] Ref. 15.

[d] Ref. 61.

[e] HFC means Hartree-Fock calculation with polarization and relation corrections included.

[f] HF means Hartree-Fock calculation.

[g] APW means augmented plane-wave calculation.

[h] Adjusted to the experimental value given in column 1.

[j] D and D' are attributed to transitions along Λ rather than at the L point. According to Ref. 17 the conduction band at L forms a local minimum and thus the gap is smaller than at the M_1 critical point along Λ.

[k] We attributed the peak in ϵ_2 to an exciton, which has a lower energy than the continuum threshold $X_5' \rightarrow X_3$ reported in Cols. 3–6.

[l] A unequivocal assignment for structures G and H is not possible on the basis of available band calculations. We give in Cols. 3–6 the energies of several critical-point transitions occurring in that range which might be responsible for the observed features.

be the subject of some controversy. The value given here is in much better agreement with the theoretical one[4] obtained with ab $initio$ calculations[16,17] than the previous value.[3-5] We also pointed out that the exciton-phonon interaction cannot be neglected in calculating the binding energy of the first exciton state.

Structures at higher energy have been assigned to M_1 critical-point transitions at L. We emphasized that the electron-hole interaction changes the expected line shape and also seems to generate a bound state. Most of the observed peaks in the case of core transitions in alkali halides have been proven recently to be excitonic.[41,60] In such

a case it was concluded that any comparison between the experimental ϵ_2 and the calculated joint density of states becomes almost meaningless. It seems that the same statement holds also for the valence-to-conduction band transitions. According to our analysis, structures in the calculated ϵ_2 originating from the joint density of states are smeared because of the electron-hole interaction, and they may not appear in the experimental ϵ_2 spectrum. Thus the important feature above the band gap is the dip at 16 eV, rather than the two broad bands peaking at 14.5 and 17.5 eV. We assigned the dip to an anti-resonance originating from an exciton bound to the
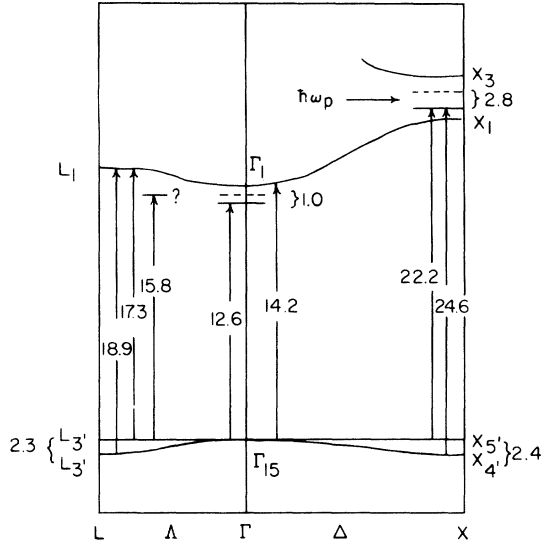
FIG. 8. Schematic energy band structure for LiF with experimental energies (eV) indicated. Solid lines denote transverse excitons; dashed lines, their longitudinal counterparts. Valence-band spin-orbit splittings (eV) are also shown.

$\Lambda_3 \rightarrow \Lambda_1$ saddle-point transitions.

We have also shown that the peak in ϵ_2 at[3] 21.7 eV is not a resonance of the electronic polaron, but that probably it corresponds to an X exciton. Finally, the differential longitudinal spectrum proved to be a powerful tool for separating and identifying structures due to plasma resonances from those due to excitonic transitions. That so many resonances occur in the 22–26 eV range strongly suggests an energy gap at X, as shown in Fig. 8. That is, X_3 probably lies above X_1.

There are still some features which we have not attempted to explain, mainly because they are not in accord with the available LiF energy bands. For the same reason, some of the assignments suggested here are only tentative and they must be confirmed by new improved calculations of the optical properties of LiF with the electron-hole and the electron-phonon interactions fully taken into account.

ACKNOWLEDGMENTS

APPENDIX

We review here the expressions for the complex dielectric function $\tilde{\epsilon}$ near an M_0 threshold when both the electron-hole interaction and a phenomenological broadening are included. A general expression for the dielectric function of an insulator, including spin degeneracy, can be written in the form

$$\epsilon(\hbar\omega) = 1 + \frac{8\pi e^2 \hbar^2}{m} \sum_l f_{l,0}\varphi_l. \tag{A1}$$

$\hbar\omega$ is the photon energy, e and m are the electron charge and rest mass, respectively, $f_{l,0}$ is the oscillator strength for a transition from the crystal ground state to a discrete state l, and φ_l is the line-shape function. We shall let l run over the set of exciton states $1, 2, \ldots, \infty$ and their continuum, corresponding to interband transitions. In the latter case, l will be identical with the crystal wave vector $\vec{k}$. In the case of a weak exciton-phonon interaction, φ_l is an asymmetric Lorentzian function, Eq. (2) of Sec. III.[37,38] For the interband transitions, φ_l will be a symmetric Lorentzian function $[E^2 - (\hbar\omega + i\Gamma)^2]^{-1}$. In the effective-mass approximation the oscillator strength is given by[23]

$$f_{l,0} = \frac{2}{3m} \frac{|\Phi_l(0)|^2 |\vec{P}_{v,c}|^2}{E_l}, \tag{A2}$$

where E_l is the energy of the lth crystal excited state referred to the ground-state energy, $\vec{P}_{v,c}$ is the dipole matrix element for transitions between the valence and the conduction band in the absence of the electron-hole interaction, $\Phi_l(\vec{r})$ is the exciton envelope function, $\vec{r}$ being the electron-hole relative coordinate. In the case of isotropic bands and allowed transitions, $|\Phi_l(0)|^2$ is

$$|\Phi_n(0)|^2 = \frac{1}{\pi n^3}\left(\frac{2\mu}{\hbar^2}\right)^{3/2} G^{3/2}, \quad n = 1, 2, \ldots, \infty \tag{A3}$$

$$|\Phi_{\vec{k}}(0)|^2 = \frac{\pi\beta e^{\pi\beta}}{\sinh(\pi\beta)}, \tag{A4}$$

for the cases of bound exciton and continuum states, respectively. In Eqs. (A3) and (A4), μ is the electron-hole reduced effective mass, G is the exciton effective Rydberg, and $\beta = [G/(E(\vec{k}) - E_g)]^{1/2}$. $E(\vec{k})$ is the valence- to conduction-band energy difference given by $E(k) = E_g + \hbar^2 k^2/2\mu$.

Substitution of Eqs. (A2), (A3), and (A4) into (A1) gives

$$\tilde{\epsilon}(\hbar\omega) = 1 + \frac{16\pi e^2 \hbar^2}{3m^2} |\vec{P}_{vc}|^2 \left[\sum_{n=1}^{\infty} \frac{G^{3/2}}{\pi n^3}\left(\frac{2\mu}{\hbar^2}\right)^{3/2} \frac{1}{\hbar\omega E_n} \frac{1 - A_n}{E_n - (\hbar\omega + i\Gamma_n)} + \sum_{\vec{k}} \frac{\pi\beta e^{\pi\beta}}{\sinh(\pi\beta)} \frac{1}{E(\vec{k})} \frac{1}{E(\vec{k})^2 - (\hbar\omega + i\Gamma)^2}\right]. \tag{A5}$$

The first term in brackets corresponds to discrete exciton transitions occurring at $E_n = E_g - G/n^2$, the second term is the interband term. In the limit of $\beta \to 0$, which means either $G \to 0$ (no electron-hole interaction) or $E(\vec{k}) \gg E_g$ (far from the interband threshold), (A4) reaches the asymptotic value of 1, and the second term in the brackets of Eq. (A5) gives the well-known expression for the dielectric function in the absence of electron-hole interaction:

$$\mathscr{E}(\hbar\omega) = 1 + \frac{4e^2\hbar^2}{3m^2}\left(\frac{2\mu}{\hbar^2}\right)^{3/2}\frac{|\vec{P}_{vc}|^2}{(\hbar\omega+i\Gamma)^2}$$

$$\times [\,2\sqrt{E_g} - (\hbar\omega+i\Gamma+E_g)^{1/2} + i(\hbar\omega+i\Gamma-E_g)^{1/2}\,].$$

(A6)

As usual, the summation over $\vec{k}$ has been transformed into an integral over E according to

$$\sum_{\vec{k}} \to \int \frac{k^2\,dk}{2\pi^2} = \frac{1}{4\pi^2}\left(\frac{2\mu}{\hbar^2}\right)^{3/2}\int_{E_g}^{\infty}(E-E_g)^{1/2}\,dE.$$

Let us define the constant factor in Eq. (A6) as the intensity K of the interband transitions:

$$K = \frac{4e^2\hbar^2}{3m^2}\left(\frac{2\mu}{\hbar^2}\right)^{3/2}|\vec{P}_{v,c}|^2.$$

(A7)

With this definition Eq. (A5) becomes

$$\mathscr{E}(\hbar\omega) = 1 + 2K\left(\frac{2G^{3/2}}{\hbar\omega}\sum_{n=1}^{\infty}\frac{1}{n^3}\frac{1}{E_n}\frac{1-iA_n}{E_n-(\hbar\omega+i\Gamma)} + G^{1/2}\int_{E_g}^{\infty}\frac{1}{1-e^{-2\pi[G/(E-E_g)]^{1/2}}}\frac{1}{E[E^2-(\hbar\omega+i\Gamma)^2]}\,dE\right) \quad \text{(A8)}$$

Equation (A8) yields both the real and the imaginary parts of the dielectric function in the case of an M_0 excitonic transition in the effective-mass approximation, and it is the basic formula used in Sec. III. The quantity σ_0 appearing in Eq. (2), corresponds to $8KG^{3/2}n^{-3}$ and, obviously, decreases as n^{-3}. However, the $n=1$ exciton state of LiF, as well as of the other alkali halides, requires central cell corrections. Since we could not calculate these corrections, in the fit of Sec. III we applied the following phenomenological procedure: We let the $n=1$ state binding energy E_b be different from the exciton Rydberg G. Accordingly, its intensity was put equal to $8KE_b^{3/2}$ instead of $8KG^{3/2}$. This is justified by the fact that the intensity for the nth state can be rewritten

as $8K(G/n^2)^{3/2}$; i.e. it can be expressed in terms of the binding energy G/n^2 of the nth state. Since $E_b > G$, the $n=1$ state has an oscillator strength larger than in the hydrogenic model.

Finally, the expected thermomodulation line shape was not calculated using Eq. (3) of Sec. III, which requires the analytical expressions for the partial derivatives $\partial\mathscr{E}/\partial E_b$ and $\partial\mathscr{E}/\partial\Gamma$. These are difficult to work with. Instead the numerical calculation was performed by calculating the difference between two $\mathscr{E}$ curves obtained applying Eq. (A8) for $E_g(\Gamma)$ and $E_g+\Delta E_g(\Gamma+\Delta\Gamma)$, respectively; i.e.,

$$\Delta\mathscr{E} = \mathscr{E}(E_g+\Delta E_g) - \mathscr{E}(E_g).$$

†Work performed for the U. S. Energy Research and Development Administration under Contract No. W-7405-eng. 82.

*Present address: Gruppo Nazionale di Struttura della Materia del C. N. R., Sezione di Roma, Istituto di Fisica dell'Università, Rome, Italy.

[1] R. Kato, J. Phys. Soc. Jpn. 16, 2525 (1961).

[2] J. C. Lemonnier, G. Stephan, and S. Robin, C. R. Acad. Sci. (Paris) 261, 2463 (1965).

[3] D. M. Roessler and W. C. Walker, J. Phys. Chem. Solids 28, 1507 (1967).

[4] G. Stephan, thesis (Rennes, 1970) (unpublished).

[5] K. Rao, thesis (University of Wisconsin, 1975) (unpublished); K. Rao, T. J. Moravec, J. C. Rife, and R. N. Dexter, Phys. Rev. B 12, 5937 (1975).

[6] A. Milgram and M. P. Givens, Phys. Rev. 125, 1506 (1962).

[7] M. Watanabe, H. Mishida, and A. Ejiri, Proceedings of the 4th International Conference on Vacuum Ultraviolet Radiation Physics, Hamburg, edited by E. E. Koch, R. Haensel, and C. Kunz (Vieweg, Braunschweig, 1974), p. 370.

[8] M. Creuzburg and H. Raether, Solid State Commun. 2, 175 (1964).

[9] O. Sueoka, J. Phys. Soc. Jpn. 20, 2226 (1965).

[10] M. Creuzburg, Z. Phys. 196, 433 (1966).

[11] C. Gout and F. Pradal, J. Phys. Chem. Solids 29, 581 (1968).

[12] See, e.g., J. C. Phillips, Solid State Phys. 18, 56 (1966).

[13] The data of Ref. 4 and Ref. 6, taken with line sources, shows some spurious fine structure not present in the data taken with continuous sources (Refs. 5 and 7).

[14]For a review of these see, e.g., Ref. 5 and also S. T. Pantelides, Phys. Rev. B **11**, 2391 (1975).

[15]R. N. Euwema, A. A. Wepfer, G. T. Surratt, and D. L. Wilhite, Phys. Rev. B **9**, 5249 (1974).

[16]F. Perrot, Phys. Status Solidi B **52**, 163 (1972).

[17]D. J. Mickish, A. B. Kunz, and T. C. Collins, Phys. Rev. B **9**, 4461 (1974).

[18]M. Piacentini, Solid State Commun. **17**, 697 (1975).

[19]W. P. Menzel, C. C. Lin, D. F. Fouquet, E. E. Lafon, and R. Chaney, Phys. Rev. Lett. **30**, 1313 (1973).

[20]C. Jouanin, J. P. Albert, and C. Gout, C. R. Acad. Sci. (Paris) B **278**, 743 (1974).

[21]T. Miyakawa, J. Phys. Soc. Jpn. **17**, 1895 (1962).

[22]J. T. Devreese, A. B. Kunz, and T. C. Collins, Solid State Commun. **11**, 673 (1972).

[23]See, e.g., R. J. Elliott, Phys. Rev. **108**, 1384 (1957).

[24]C. G. Olson, M. Piacentini, and D. W. Lynch, Phys. Rev. Lett. **33**, 644 (1974).

[25]J. H. Weaver, C. G. Olson, D. W. Lynch, and M. Piacentini, Solid State Commun. **16**, 163 (1975).

[26]D. E. Aspnes and C. G. Olson, Phys. Rev. Lett. **33**, 1605 (1974).

[27]M. Cardona, *Modulation spectroscopy* (Academic, New York, 1969), p. 118.

[28]C. G. Olson and D. W. Lynch, Phys. Rev. B **9**, 3159 (1974).

[29]This relation also establishes the sign of our differential spectra, $\Delta R = R(T + \Delta T) - R(T)$.

[30]L. Nosenzo, E. Reguzzoni, and G. Samoggia, Phys. Rev. Lett. **28**, 1388 (1972).

[31]A. Balzarotti, E. Colavita, S. Gentile, and R. Rosei, Appl. Opt. **14**, 2412 (1975).

[32]T. Tomiki and T. Miyata, J. Phys. Soc. Jpn. **27**, 658 (1969).

[33]The scaling of σ_0 is required to bring the calculated $\Delta\epsilon_2$ in agreement with the experimental one. It is not a different normalization of the TM spectra, to agree with our data above 13.6 eV.

[34]M. Menes, Phys. Rev. B **10**, 4469 (1974).

[35]Y. Toyozawa, M. Inoue, T. Inui, and E. Hanamura, J. Phys. Soc. Jpn. **22**, 1337, 1349 (1967).

[36]S. Antoci and G. F. Nardelli, Surf. Sci. **37**, 836 (1973).

[37]Y. Toyozawa, Prog. Theor. Phys. **20**, 53 (1958).

[38]H. Sumi, J. Phys. Soc. Jpn. **82**, 616 (1972).

[39]The thermal shift of the band gap and the excitons to higher energies upon cooling occurs in almost every material with a direct band gap at the center of the Brillouin zone. Part of this shift is due to lattice dilatation and this contribution can be obtained from hydrostatic pressure experiments. Another part of the shift is due to the exciton-phonon interaction under discussion. In the few cases where hydrostatic pressure data are available, it has been possible to determine that the two processes give comparable contributions to the temperature coefficient of the band gap. See, e.g. D. W. Lynch and A. D. Brothers, Phys. Rev. Lett. **21**,

689 (1968) and A. D. Brothers and D. W. Lynch, Phys. Rev. **180**, 911 (1969).

[40]B. Batz, Semiconductors and Semimetals **9**, 315 (1972) and references therein.

[41]W. Gudat, C. Kunz and H. Petersen, Phys. Rev. Lett. **32**, 1370 (1974).

[42]S. P. Kowalczyk, F. R. McFeely, L. Ley, R. A. Pollak, and D. A. Shirley, Phys. Rev. B **9**, 3573 (1974).

[43]The energy bands of LiF have been calculated for different values of the lattice constant by Euwema *et al.* (Ref. 15), in order to obtain the equilibrium properties of the crystal. We are very grateful to Dr. Euwema for supplying us with the detailed results of the calculations not given in Ref. 15. According to their calculations, the valence-to-conduction band energy gaps decrease almost rigidly as the lattice constant increases, with different coefficients for each different pair of bands. It must be noted, however, that in several alkali halides the energy of transitions at X decreases with decreasing lattice constant (see papers cited in Ref. 39). Calculations on KI [A. B. Kunz, J. Phys. Chem. Solids **31**, 265 (1970)] confirmed this experimental result and also showed that the energy of transitions at L depends slightly on the lattice constant. The interpretation suggested in the text for the structures found between 15 and 20 eV is based on the results of Euwema *et al.* (Ref. 15), but we feel that further theoretical as well as experimental investigation is required.

[44]B. Velicky and J. Sak, Phys. Status Solidi **16**, 147 (1966).

[45]U. Fano, Phys. Rev. **124**, 1866 (1961).

[46]K. P. Jain, Phys. Rev. **139**, A544 (1965).

[47]Y. Onodera, *Proceedings of the 3rd International Conference on Vacuum Ultraviolet Radiation Physics Tokyo, 1971*, edited by Y. Nakai (Physical Society of Japan, Tokyo, 1971), p. B2-1.

[48]Y. Onodera, Phys. Rev. B **4**, 2751 (1971).

[49]J. C. Hermanson, Phys. Rev. **177**, 1234 (1966).

[50]Y. Toyozawa, Prog. Theor. Phys. **12**, 421 (1954).

[51]A. B. Kunz, J. T. Devreese, and T. C. Collins J. Phys. C **5**, 3259 (1972).

[52]G. J. Lapeyre, J. Anderson, J. A. Knapp, and P. L. Gobby, Phys. Rev. Lett. **33**, 1290 (1974).

[53]G. Baldini and B. Bosacchi, Phys. Rev. **166**, 863 (1968).

[54]G. W. Rubloff, Phys. Rev. B **5**, 662 (1972).

[55]T. Miyakawa, J. Phys. Soc. Jpn. **24**, 768 (1968).

[56]R. S. Knox, *Theory of Excitons* (Academic, New York, 1963).

[57]S. L. Adler, Phys. Rev. **126**, 413 (1962).

[58]M. Piacentini, Nuovo Cimento B **63**, 458 (1969).

[59]D. W. Lynch, M. Piacentini, and C. G. Olson, Phys. Rev. Lett., **35**, 1658 (1975).

[60]For a review of these see, e.g., Ref. 5 and also, S. T. Pantelides, Phys. Rev. B **11**, 2391 (1975).

[61]G. E. Laramore and A. C. Switendick, Phys. Rev. B **7**, 3615 (1973).